

## A New Global Solar-induced Chlorophyll Fluorescence (SIF) Data Product from TanSat Measurements

Lu YAO<sup>1,2</sup>, Dongxu YANG<sup>1,3</sup>, Yi LIU<sup>1,3</sup>, Jing WANG<sup>1,2</sup>, Liangyun LIU<sup>4</sup>, Shanshan DU<sup>2,4</sup>, Zhaonan CAI<sup>1</sup>, Naimeng LU<sup>5</sup>, Daren LYU<sup>1</sup>, Maohua WANG<sup>3</sup>, Zengshan YIN<sup>7</sup>, and Yuquan ZHENG<sup>6</sup>

<sup>1</sup>Key Laboratory of Middle Atmosphere and Global Environment Observation, Institute of Atmospheric Physics, Chinese Academy of Sciences, Beijing 100029, China

<sup>2</sup>University of Chinese Academy of Sciences, Beijing 100049, China

<sup>3</sup>Shanghai Advanced Research Institute, Chinese Academy of Sciences, Shanghai 201210, China

<sup>4</sup>Key Laboratory of Digital Earth Science, Institute of Remote Sensing and Digital Earth, Chinese Academy of Sciences, Beijing 100094, China

<sup>5</sup>National Satellite Meteorological Center, China Meteorological Administration, Beijing 100081, China

<sup>6</sup>Changchun Institute of Optics, Fine Mechanics and Physics, Changchun 130033, China

<sup>7</sup>Shanghai Engineering Center for Microsatellites, Shanghai 201210, China

(Received 30 July 2020; revised 19 November 2020; accepted 2 December 2020)

### ABSTRACT

The Chinese Carbon Dioxide Observation Satellite Mission (TanSat) is the third satellite for global CO<sub>2</sub> monitoring and is capable of detecting weak solar-induced chlorophyll fluorescence (SIF) signals with its advanced technical characteristics. Based on the Institute of Atmospheric Physics Carbon Dioxide Retrieval Algorithm for Satellite Remote Sensing (IAPCAS) platform, we successfully retrieved the TanSat global SIF product spanning the period of March 2017 to February 2018 with a physically based algorithm. This paper introduces the new TanSat SIF dataset and shows the global seasonal SIF maps. A brief comparison between the IAPCAS TanSat SIF product and the data-driven SVD (singular value decomposition) SIF product is also performed for follow-up algorithm optimization. The comparative results show that there are regional biases between the two SIF datasets and the linear correlations between them are above 0.73 for all seasons. The future SIF data product applications and requirements for SIF space observation are discussed.

**Key words:** TanSat, solar-induced chlorophyll fluorescence, retrieval algorithm, remote sensing

**Citation:** Yao, L., and Coauthors, 2021: A new global Solar-induced Chlorophyll Fluorescence (SIF) data product from TanSat measurements. *Adv. Atmos. Sci.*, **38**(3), 341–345, <https://doi.org/10.1007/s00376-020-0204-6>.

---

## 1. Global SIF observations from space

The carbon cycle between the atmosphere and the terrestrial ecosystem plays an important role in climate change. Reliable and accurate assessment of the gross primary production (GPP) of vegetation is critical in determining the surface carbon flux and understanding climate feedback. Solar-induced chlorophyll fluorescence (SIF) is widely recognized as the ideal proxy for plant GPP because it represents an electromagnetic emission that is directly linked to photosynthetic activity (Frankenberg et al., 2011a; Guanter et al., 2012, 2014; Zhang et al., 2014; Yang et al., 2015b; Sun et al., 2017; Frankenberg and Berry, 2018; MacBean et al., 2018). Studies have shown a strong linear correlation between SIF and GPP on large spatial scales (Guanter et al., 2012; Frankenberg and Berry, 2018). Since the first successful attempt at measuring SIF from the Medium Resolution Imaging Spectrometer (MERIS) onboard the ENVironmental SATellite (ENVISAT) (Guanter et al., 2007), the measurement of SIF signals from space has drastically improved global spatial coverage. Hyperspectral instruments that measure the O<sub>2</sub>-A band onboard the new generation of greenhouse gas satellites, such as the Greenhouse Gases Observing Satellite (GOSAT) from Japan (Frankenberg et al., 2011a; Joiner et al., 2011) and the Orbiting Carbon Observat-

---

\* Corresponding author: Jing WANG  
Email: [jingwang@mail.iap.ac.cn](mailto:jingwang@mail.iap.ac.cn)

ory 2 (OCO-2) from the U.S., provide new global SIF observations that approached from the in-filling effect of solar Fraunhofer lines. Medium spectral resolution instruments for monitoring atmospheric trace gases, such as the Global Ozone Monitoring Experiment-2 (GOME-2), are also capable of detecting SIF signals from space (Joiner et al., 2013; Köhler et al., 2015). Furthermore, the European satellite mission TROPospheric Monitoring Instrument (TROPOMI) started an imaging observation of SIF in October 2017 (Köhler et al., 2018; Sun et al., 2018). The Chinese global carbon dioxide monitoring satellite (TanSat) was launched successfully in December 2016 (Chen et al., 2012; Ran and Li, 2019) and became the third greenhouse gas satellite for CO<sub>2</sub> monitoring (Liu et al., 2018; Yang et al., 2018). TanSat moves in a sun-synchronous orbit crossing the equator at about 1330 LST (LST=UTC+8) with a 16-day repeat cycle (Liu et al., 2018). The TanSat mission was supported by the Ministry of Science and Technology of China, the Chinese Academy of Sciences, and the China Meteorological Administration. The Atmospheric Carbon-dioxide Grating Spectroradiometer (ACGS), the main instrument of TanSat, measures the O<sub>2</sub>-A band with a spectral resolution of 0.039–0.042 nm and covers a spectral range of 758–778 nm (Wang et al., 2014; Li et al., 2017; Zhang et al., 2017). The measurement outside the strong O<sub>2</sub> absorption lines in this band was used to approach SIF in this study. There are nine footprints across the track of TanSat on the ground in a frame, and the nadir footprint is about the size of 2 km × 2 km.

## 2. SIF approaching from TanSat measurement

The first TanSat global SIF map and data product originated from a data-driven algorithm based on singular value decomposition (SVD) techniques and has been introduced in a previous study (Du et al., 2018). In the data-driven algorithm, the measured spectrum is expressed as a linear combination of the SIF signal and several singular vectors that are trained with non-vegetated samples. This approach calculates the radiance contribution of SIF emission with a linear least-squares fitting, which is efficient in global retrievals and has been applied in GOSAT, OCO-2, and TROPOMI SIF retrievals (Guanter et al., 2012; Frankenberg et al., 2014; Köhler et al., 2018). The systematic error is removed during the training process. However, unexpected errors might arise due to the imperfect training dataset and varied measurement errors. The physical-based retrieval method is well-known as a highly accurate approach because it simulates the radiative transfer in the atmosphere between the surface and satellite. Differential Optical Absorption Spectroscopy (DOAS) techniques have also been used in OCO-2 official SIF product retrieval (Frankenberg, 2014).

In this study, we introduce a new TanSat SIF product that is approached by a DOAS based retrieval algorithm developed from the Institute of Atmospheric Physics Carbon Dioxide Retrieval Algorithm for Satellite Remote Sensing (IAP-CAS) (Yang et al., 2015a). The IAPCAS has been developed and applied in TanSat XCO<sub>2</sub> retrieval (Liu et al., 2018; Yang et al., 2018) and provides a well-developed forward model that contains both atmosphere and surface models (Liu et al., 2013). The study indicated that atmospheric scattering had only a limited impact on the SIF signal at the top of the atmospheric (TOA) (Frankenberg et al., 2011b); hence, only the extinction of light along the path was considered, and the Beer-Lambert Law was applied in the forward model instead of the full radiative transfer model. The forward model  $f$  can be written as

$$f(F_{s,rel}, \mathbf{a}) = \ln(\langle \mathbf{I}_t + F_{s,rel} \mathbf{I} \rangle) + \sum_{i=0}^n a_i \lambda^i,$$

in which  $\mathbf{I}_t$  is the normalized, disk-integrated solar transmission spectrum,  $\mathbf{I}$  is a unit vector,  $F_{s,rel}$  is the relative SIF signal corresponding to the continuum level radiance in the 757-nm micro-window (758.4–759.2 nm), and the convolution operator  $\langle \rangle$  converts the spectrum of high-resolution to instrument resolution using the instrument line shape. The retrieved parameter  $\mathbf{a}$  consists of three polynomial coefficients ( $a_i, i = 0, 1, 2$ ) which serves to model the continuum level radiance in the wavelength  $\lambda$ . The far-wings effect of the O<sub>2</sub> lines has a minimal impact upon the continuum level radiance but is still considered in the retrieval to optimize the fit. In summary, the state vector list includes the relative SIF signal, the O<sub>2</sub> column absorption factor, wavelength grid shift, and the coefficients of a second-order polynomial that approximates the continuum level radiance. A non a priori constrained Gaussian-Newton method is used in the inversion process, where the measurement noise was also considered. The SIF at TOA is calculated by multiplying the retrieved relative SIF with the continuum level radiance in the micro-window. The measurements over desert, snow, and bare soil are considered to have no SIF emission and are used in bias correction to reduce measurement systematic error. We use a daily varied bias correction for each footprint, and the bias is also calculated with the measurement continuum level radiance. In our data product, we provide both the bias-corrected and the raw retrieved SIF.

The SIF data product for future analysis should undergo the cloud-filter and have good fitting quality. The continuum coverage, the range of the solar zenith angle, and the root mean square (RMS) of the spectrum fitting residual is used in the post-screening process for quality control.

Before applied to TanSat measurements, the IAPCAS/SIF retrieval algorithm was used to obtain the SIF results from

OCO-2 observations to test the algorithm. The results show good agreement between the OCO-2 IAPCAS/SIF retrieval and the OCO-2 official product (OCO2\_Level 2\_Lite\_SIF.8r) with the coefficient of determination ( $R^2$ ) of 0.86, a root mean square error (RMSE) of  $0.19 \text{ W m}^{-2} \mu\text{m}^{-1} \text{ sr}^{-1}$ .

The limited ground-based SIF measurements and the spatial-scale differences between the SIF from canopy observations and those derived from space make it difficult to validate the retrieved SIF of a single sounding, while the SIF uncertainty for each grid-cell could be calculated for further applications. The grid-cell SIF uncertainty is reduced by the multi-soundings within the grid and is much lower than the precision of a single measurement that is dominated by instrumental noise (Sun et al., 2018). In Fig. 1, the seasonal TanSat SIF product for 757 nm (March 2017–February 2018) retrieved from the IAPCAS/SIF algorithm is shown. From the global SIF maps, it is clear that the IAPCAS/SIF dataset shows the SIF signal of the large vegetation areas, e.g., Southeast China, South Asia, Europe, the rainforests in Africa, and the Amazon, and the eastern US. The seasonal variation in deciduous forests and grassland was consistent with the vegetative growing state, throughout the year, which has also been observed by the GOSAT and OCO-2 SIF products (Frankenberg et al., 2014; Frankenberg and Berry, 2018; Sun et al., 2018; Somkuti et al., 2020). This new TanSat SIF product derived from the IAPCAS/SIF algorithm is archived on International Reanalysis Cooperation on Carbon Satellites Data (IRCSD) and will be accessible to the public when this paper is published ([www.chinageoss.org/tansat](http://www.chinageoss.org/tansat)), as well as the OCO-2 SIF data product with the IAPCAS/SIF algorithm.

The SIF products from IAPCAS/SIF and SVD data-driven retrieval show obvious bias in the global maps (Figs. 1e–h). SIF retrieved with IAPCAS/SIF algorithm has a large global negative bias in spring (MAM) and summer (JJA), but this

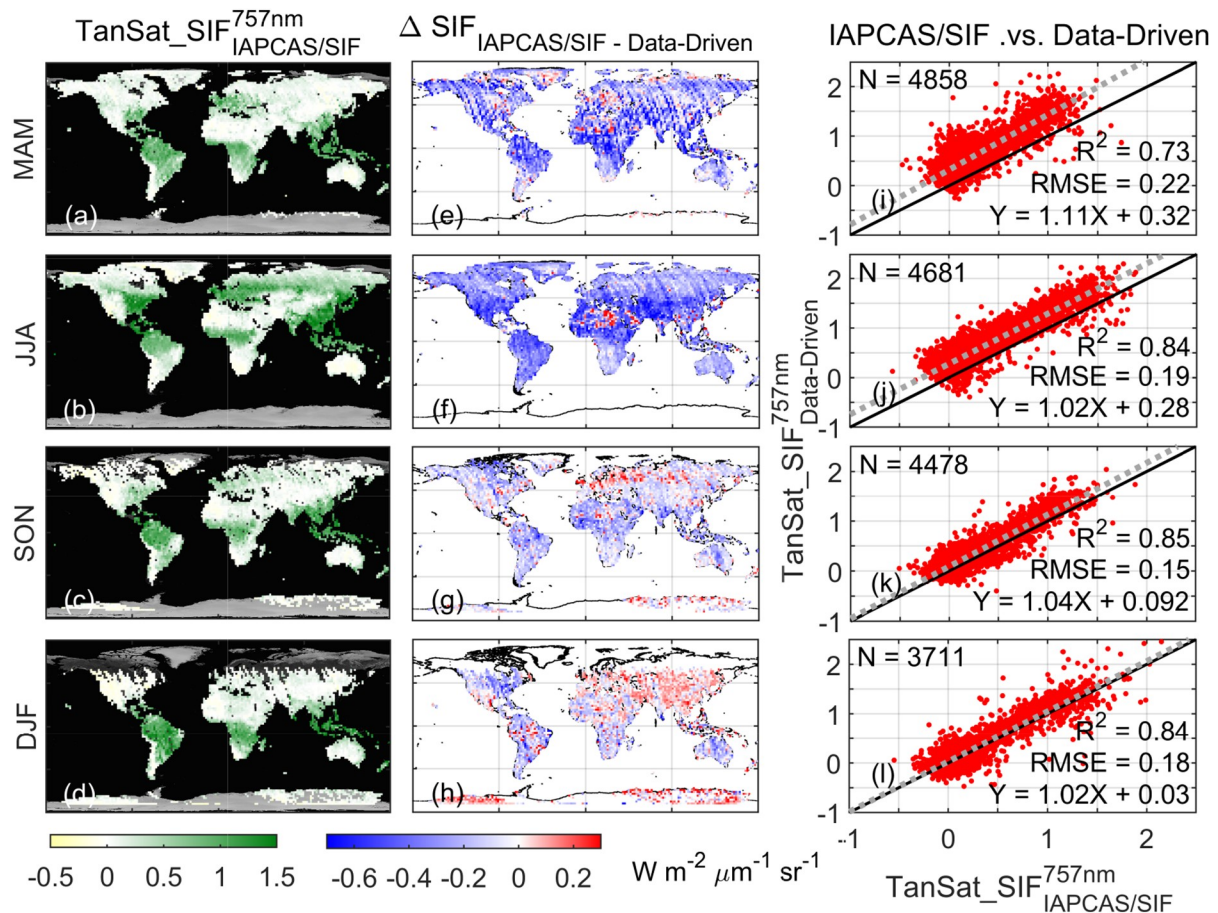


**Fig. 1.** Seasonal global SIF map and the differences between the IAPCAS/SIF and SVD data-driven SIF products. All subplots are shown based on  $2^\circ \times 2^\circ$  grid data, and all soundings in each grid were used to obtain the average SIF value for each grid. The rows of subplots indicate spring (MAM), summer (JJA), fall (SON), and winter (DJF) in the Northern Hemisphere from top to bottom. The seasonally averaged SIF distributions of TanSat from March 2017 to February 2018 are shown in the left column (a–d). The subplots (e–h) are the SIF differences between the two SIF products for each season. The seasonally averaged TanSat SIF from the two algorithms is also shown in a scatterplot in the right column (i–l) with statistics in each subplot. The scatter plots show that the two products agree well at the seasonal temporal scale, with the RMSE of less than  $0.22 \text{ W m}^{-2} \mu\text{m}^{-1} \text{ sr}^{-1}$  and the  $R^2$  larger than 0.73 for all seasons. The fitting function and the grid number for the statistic are also indicated in subplots.

bias is much smaller in the fall (SON) and winter (DJF). This bias could be caused by the differences in retrieval methods, especially the methods that are used to select the non-SIF emission measurements. In the data-driven algorithm, a training dataset of no SIF emission measurements has been selected to represent the background signal. The MODIS nadir BRDF-adjusted reflectance product MCD43C4 (0.05 degree, <http://doi.org/10.5067/MODIS/MCD43C4.006>) is used in this selection (Du et al., 2018). In the IAPCAS/SIF algorithm, the MODIS land cover type product MCD12C1 (0.05 degree, <https://doi.org/10.5067/MODIS/MCD12C1.006>) has been used in the no SIF emission measurements selection and the no SIF emission measurement solely works in the bias correction process. The main purpose of the selection is to find a reference that represents the measurement without any SIF signal. This is justified because the SIF signal is very weak and the instrument issue (e.g. radiometric calibration and stray light) could introduce a spurious SIF-like signal. Therefore, the two algorithms make two different no SIF emission datasets to provide references, which finally causes bias. The data-driven retrieval reference to the measurement lets the retrieval procedure reduce the instrument impact in the training process, but the IAPCAS/SIF reference to a theoretical model can only correct the instrument issues in the bias correction process. Therefore the IAPCAS/SIF is indeed more sensitive to the measurement (spectrum) quality than data-driven retrieval. The scatterplots demonstrate the grid-cell inter-comparison between the two SIF products (Figs. 1i–l), and they maintain a strong linear relationship over all four seasons with the RMSE less than  $0.22 \text{ W m}^{-2} \mu\text{m}^{-1} \text{ sr}^{-1}$ . The worst linear correlation between the two products appears in spring with an  $R^2$  of 0.73 while the  $R^2$  for other seasons is about 0.84.

### 3. Outlook

Many satellite missions that have the capability to measure SIF, including GOSAT (-2), OCO-2 (-3), TanSat, and TROPOMI, have been launched in recent years. The global coverage of SIF measurements will be significantly improved as long as all satellite missions provide data products with similar quality. The data product quality, evaluated according to both accuracy and precision, is one of the key issues we need to investigate before applying the product to the carbon cycle and climate research, further noting that this depends on measurement processing, e.g., instrument performance and retrieval algorithm development. In addition, the satellite measured instantaneous SIF signal was directly linked to vegetation photosynthesis, which means that multiple factors, e.g., incoming sunlight, growing status of vegetation, and observation geometry, have a series of potential impacts on the detected SIF signal. The method for using this instantaneous measurement in model or data assimilation studies needs to be investigated. The application of SIF data in "top-down" carbon flux inversion can significantly improve the uncertainty of the estimated carbon sinks (vegetation) in the land-atmosphere carbon exchange process and consequently provide an opportunity to advance the understanding of anthropogenic emissions of greenhouse gases. Future missions, including the European Space Agency (ESA) FLuorescence EXplorer (FLEX), which will be launched in 2024 (Drusch et al., 2017), and TanSat-2, which is currently in the pre-design phase, will provide more advantageous SIF measurements that will contribute to research on the climate and the global carbon cycle.

**Acknowledgements.** This study was supported by the National Key R&D Program of China (No. 2016YFA0600203), the Key Research Program of the Chinese Academy of Sciences (ZDRW-ZS-2019-1 & ZDRW-ZS-2019-2), and the Youth Program of the National Natural Science Foundation of China (41905029). The TanSat L1B data service was provided by the International Reanalysis Cooperation on Carbon Satellite Data (IRCS) (131211KYSB20180002) and the Cooperation on the Analysis of Carbon Satellite Data (CASA). The authors thank the OCO-2 team for providing the Level-2 SIF data products.

**Electronic supplementary material:** Supplementary material is available in the online version of this article at <https://doi.org/10.1007/s00376-020-0204-6>.

### REFERENCES

- Chen, W., Y. H. Zhang, Z. S. Yin, Y. Q. Zheng, C. X. Yan, Z. D. Yang, and Y. Liu, 2012: The TanSat mission: Global CO<sub>2</sub> observation and monitoring. Proceedings of the 63rd International Astronautical Congress, Naples, Italy, International Astronautical Federation.
- Drusch, M., and Coauthors, 2017: The fluorescence EXplorer mission concept-ESA's earth Explorer 8. *IEEE Trans. Geosci. Remote Sens.*, **55**, 1273–1284, <https://doi.org/10.1109/TGRS.2016.2621820>.
- Du, S. S., L. Y. Liu, X. J. Liu, X. Zhang, X. Y. Zhang, Y. M. Bi, and L. C. Zhang, 2018: Retrieval of global terrestrial solar-induced chlorophyll fluorescence from TanSat satellite. *Science Bulletin*, **63**(22), 1502–1512, <https://doi.org/10.1016/j.scib.2018.10.003>.
- Frankenberg, C., 2014: D-81519 OCO-2 Algorithm Theoretical Basis Document IMAP-DOAS preprocessor. California Institute of Technology, California.
- Frankenberg, C., and J. Berry, 2018: 3. 10 - Solar induced chlorophyll fluorescence: Origins, relation to photosynthesis and retrieval. *Comprehensive Remote Sensing*, **3**, 143–162, <https://doi.org/10.1016/B978-0-12-409548-9.10632-3>.
- Frankenberg, C., and Coauthors, 2011a: New global observations of the terrestrial carbon cycle from GOSAT: Patterns of plant fluorescence with gross primary productivity. *Geophys. Res. Lett.*, **38**, L17706, <https://doi.org/10.1029/2011GL048738>.

- Frankenberg, C., A. Butz, and G. C. Toon, 2011b: Disentangling chlorophyll fluorescence from atmospheric scattering effects in O<sub>2</sub> A-band spectra of reflected sun-light. *Geophys. Res. Lett.*, **38**(3), L03801, <https://doi.org/10.1029/2010GL045896>.
- Frankenberg, C., C. O'Dell, J. Berry, L. Guanter, J. Joiner, P. Köhler, R. Pollock, and T. E. Taylor, 2014: Prospects for chlorophyll fluorescence remote sensing from the Orbiting Carbon Observatory-2. *Remote Sensing of Environment*, **147**, 1–12, <https://doi.org/10.1016/j.rse.2014.02.007>.
- Guanter, L., L. Alonso, L. Gómez-Chova, J. Amorós-López, J. Vila, and J. Moreno, 2007: Estimation of solar-induced vegetation fluorescence from space measurements. *Geophys. Res. Lett.*, **34**(8), L08401, <https://doi.org/10.1029/2007GL029289>.
- Guanter, L., C. Frankenberg, A. Dudhia, P. E. Lewis, J. Gómez-Dans, A. Kuze, H. Suto, and R. G. Grainger, 2012: Retrieval and global assessment of terrestrial chlorophyll fluorescence from GOSAT space measurements. *Remote Sensing of Environment*, **121**, 236–251, <https://doi.org/10.1016/j.rse.2012.02.006>.
- Guanter, L., and Coauthors, 2014: Global and time-resolved monitoring of crop photosynthesis with chlorophyll fluorescence. *Proceedings of the National Academy of Sciences of the United States of America*, **111**(14), E1327–E1333, <https://doi.org/10.1073/pnas.1320008111>.
- Joiner, J., Y. Yoshida, A. P. Vasilkov, Y. Yoshida, L. A. Corp, and E. M. Middleton, 2011: First observations of global and seasonal terrestrial chlorophyll fluorescence from space. *Biogeosciences*, **8**, 637–651, <https://doi.org/10.5194/bg-8-637-2011>.
- Joiner, J., and Coauthors, 2013: Global monitoring of terrestrial chlorophyll fluorescence from moderate-spectral-resolution near-infrared satellite measurements: Methodology, simulations, and application to GOME-2. *Atmospheric Measurement Techniques*, **6**, 2803–2823, <https://doi.org/10.5194/amt-6-2803-2013>.
- Köhler, P., L. Guanter, and J. Joiner, 2015: A linear method for the retrieval of sun-induced chlorophyll fluorescence from GOME-2 and SCIAMACHY data. *Atmospheric Measurement Techniques*, **8**, 2589–2608, <https://doi.org/10.5194/amt-8-2589-2015>.
- Köhler, P., C. Frankenberg, T. S. Magney, L. Guanter, J. Joiner, and J. Landgraf, 2018: Global retrievals of solar-induced chlorophyll fluorescence with TROPOMI: First results and inter-sensor comparison to OCO-2. *Geophys. Res. Lett.*, **45**, 10 456–10 463, <https://doi.org/10.1029/2018GL079031>.
- Li, Z. G., and Coauthors, 2017: Pre-launch spectral calibration of a carbon dioxide spectrometer. *Measurement Science and Technology*, **28**, 065801, <https://doi.org/10.1088/1361-6501/aa6507>.
- Liu, Y., D. X. Yang, and Z. N. Cai, 2013: A retrieval algorithm for TanSat XCO<sub>2</sub> observation: Retrieval experiments using GOSAT data. *Chinese Science Bulletin*, **58**(13), 1520–1523, <https://doi.org/10.1007/s11434-013-5680-y>.
- Liu, Y., and Coauthors, 2018: The TanSat mission: Preliminary global observations. *Science Bulletin*, **63**(18), 1200–1207, <https://doi.org/10.1016/j.scib.2018.08.004>.
- MacBean, N., and Coauthors, 2018: Strong constraint on modelled global carbon uptake using solar-induced chlorophyll fluorescence data. *Scientific Reports*, **8**, 1973, <https://doi.org/10.1038/s41598-018-20024-w>.
- Ran, Y. H., and X. Li, 2019: TanSat: A new star in global carbon monitoring from China. *Science Bulletin*, **64**(5), 284–285, <https://doi.org/10.1016/j.scib.2019.01.019>.
- Somkuti, P., H. Bösch, L. Feng, P. I. Palmer, R. J. Parker, and T. Quaife, 2020: A new space-borne perspective of crop productivity variations over the US Corn Belt. *Agricultural and Forest Meteorology*, **281**, 107826, <https://doi.org/10.1016/j.agrformet.2019.107826>.
- Sun, Y., and Coauthors, 2017: OCO-2 advances photosynthesis observation from space via solar-induced chlorophyll fluorescence. *Science*, **358**, eaam5747, <https://doi.org/10.1126/science.aam5747>.
- Sun, Y., C. Frankenberg, M. Jung, J. Joiner, L. Guanter, P. Köhler, and T. Magney, 2018: Overview of Solar-Induced chlorophyll Fluorescence (SIF) from the Orbiting Carbon Observatory-2: Retrieval, cross-mission comparison, and global monitoring for GPP. *Remote Sensing of Environment*, **209**, 808–823, <https://doi.org/10.1016/j.rse.2018.02.016>.
- Wang, Q., Z. D. Yang, and Y. M. Bi, 2014: Spectral parameters and signal-to-noise ratio requirement for TanSat hyper spectral remote sensor of atmospheric CO<sub>2</sub>. Proc. SPIE 9259, Remote Sensing of the Atmosphere, Clouds, and Precipitation V, 92591T (8 November 2014); <https://doi.org/10.1117/12.2067572>
- Yang, D. X., Y. Liu, Z. N. Cai, J. B. Deng, J. Wang, and X. Chen, 2015a: An advanced carbon dioxide retrieval algorithm for satellite measurements and its application to GOSAT observations. *Science Bulletin*, **60**, 2063–2066, <https://doi.org/10.1007/s11434-015-0953-2>.
- Yang, D. X., Y. Liu, Z. N. Cai, X. Chen, L. Yao, and D. R. Lyu, 2018: First global carbon dioxide maps produced from TanSat measurements. *Adv. Atmos. Sci.*, **35**(6), 621–623, <https://doi.org/10.1007/s00376-018-7312-6>.
- Yang, X., and Coauthors, 2015b: Solar-induced chlorophyll fluorescence that correlates with canopy photosynthesis on diurnal and seasonal scales in a temperate deciduous forest. *Geophys. Res. Lett.*, **42**, 2977–2987, <https://doi.org/10.1002/2015GL063201>.
- Zhang, H., Y. Q. Zheng, C. Lin, W. Q. Wang, Q. Wang, and S. Li, 2017: Laboratory spectral calibration of TanSat and the influence of multiplex merging of pixels. *Int. J. Remote Sens.*, **38**, 3800–3816, <https://doi.org/10.1080/01431161.2017.1306142>.
- Zhang, Y. G., and Coauthors, 2014: Estimation of vegetation photosynthetic capacity from space-based measurements of chlorophyll fluorescence for terrestrial biosphere models. *Global Change Biology*, **20**(12), 3727–3742, <https://doi.org/10.1111/gcb.12664>.